Published in final edited form as:
J Med Chem. 2013 May 23; 56(10): 4017–4027. doi:10.1021/jm400231v.

Extreme multidrug resistant HIV-1 protease with 20 mutations is resistant to novel protease inhibitors with P1′-pyrrolidinone or P2-*tris*-tetrahydrofuran

Johnson Agniswamy[a], **Chen-Hsiang Shen**[a], **Yuan-Fang Wang**[a], **Arun K. Ghosh**[b], **Kalapala Venkateswara Rao**[b], **Chun-Xiao Xu**[b], **Jane M. Sayer**[c], **John M. Louis**[c], and **Irene T. Weber**[a,*]

[a]Department of Biology, Molecular Basis of Disease Program, Georgia State University, Atlanta, GA30303

[b]Department of Chemistry and Medicinal Chemistry, Purdue University, West Lafayette, Indiana 47907

[c]Laboratory of Chemical Physics, National Institute of Diabetes and Digestive and Kidney Diseases, National Institutes of Health, DHHS, Bethesda, Maryland 20892-0520

Abstract

Extreme drug resistant mutant of HIV-1 protease (PR) bearing 20 mutations (PR20) has been studied with the clinical inhibitor amprenavir (**1**) and two potent antiviral investigational inhibitors GRL-02031 (**2**) and GRL-0519 (**3**). Clinical inhibitors are >1000-fold less active on PR20 than on wild type enzyme, which is consistent with dissociation constants (K_L) from isothermal titration calorimetry of 40 nM for **3**, 178 nM for amprenavir, and 960 nM for **2**. High resolution crystal structures of PR20-inhibitor complexes revealed altered interactions compared with the corresponding wild-type PR complexes in agreement with relative inhibition. Amprenavir lacks interactions due to PR20 mutations in the S2/S2′ subsites relative to PR. Inhibitors **2** and **3** lose interactions with Arg8′ in PR20 relative to the wild type enzyme since Arg8′ shifts to interact with mutated L10F side chain. Overall, inhibitor **3** compares favorably with darunavir in affinity for PR20 and shows promise for further development.

Keywords

HIV/AIDS; aspartic protease; X-ray crystallography; drug resistance

INTRODUCTION

The introduction of combination therapy, also known as highly active antiretroviral therapy (HAART), has greatly improved the outcome of HIV/AIDS therapy.[1] However, the major challenge for the success of current treatment is the emergence of drug resistant strains due to the high mutational rate caused by the infidelity of HIV reverse transcriptase.[2–4] Greater transmission by drug resistant HIV strains has been recorded in several regions around the world underscoring the therapeutic challenge.[5–11] Resistance testing is now recommended

*Corresponding Author: Phone: 404 413-5411; FAX: 404 413-5301; iweber@gsu.edu.

PROTEIN DATA BANK

Crystallographic data are available for inhibitor complexes: PR20-APV (PDB ID: 4J5J), PR20-GRL0519 (PDB ID: 4J54), PR20-GRL02031 (PDB ID: 4J55).

SUPPORTING INFORMATION AVAILABLE

Figures comparing PR20 and wild-type PR structures. This material is available free of charge via the Internet at http://pubs.acs.org.

for patients in therapy.[12] With the Treatment 2.0 initiative by UNAIDS secretariat and the World Health Organization, millions of infected people will initiate or be maintained on antiretroviral therapy.[11] Furthermore, prevention strategies using antiviral drugs have the potential to increase the prevalence of HIV drug resistant strains.[13–14] More than ever, there is an urgent demand for renewed efforts to design potent inhibitors targeting the resistant viral strains.

Recently, we characterized a clinically derived HIV-1 protease (PR20) bearing 20 mutations [Q7K, L10F, I13V, I15V, D30N, V32I, L33F, E35D, M36I, S37N, I47V, I54L, Q58E, I62V, L63P, A71V, I84V, N88D, L89T and L90M] and extremely resistant to all clinical protease inhibitors (PIs).[15–16] The inhibitor dissociation constants (K_L) of PR20 for darunavir, which was approved in 2006 for patients infected by drug resistant strains, and for saquinavir were increased by more than 8000- and 2000-fold, respectively.[15] Thermal stability studies by DSC showed that the PIs stabilize the ternary complex of PR20 (dimer+PI) to a significantly lesser extent than for PR. In addition, the critical autocatalytic cleavage of a PR20 precursor, which is required to release fully active PR, was unresponsive to all clinical PI's, whereas the autoprocessing of wild-type precursor is inhibited by darunavir and saquinavir. Recent crystallographic studies of PR20 by itself and in complexes with darunavir, saquinavir and a substrate analog that mimics the p2-NC natural cleavage site in the Gag-Pol polyprotein revealed distinct conformations for its highly flexible flaps.[16] PR20 forms six fewer hydrogen bonds with the substrate analog relative to the wild-type PR emphasizing its weak affinity. Further, PR20 mutations result in an expanded S2/S2′ binding pocket and diminished interactions with inhibitors in agreement with the lower affinity relative to wild-type PR.[15–16] These observations demonstrate that PR20 is a highly evolved drug resistant mutant, and may prove invaluable as a model system in the quest to design potent inhibitors against multidrug resistant viral strains.

Amprenavir (inhibitor **1**; Figure 1A) is a nonpeptide N, N-disubstituted amino-sulfonamide protease inhibitor approved for HIV/AIDS therapy in 1999.[17] Amprenavir shares a hydroxyethylamine core with other inhibitors such as saquinavir, but the sulfonamide group increases its solubility over saquinavir which enhances oral bioavailability.[18] Recently, two new potent antiviral inhibitors of HIV PR derived on the darunavir scaffold were reported: GRL-02031 (**2**; Figure 1B) and GRL-0519 (**3;** Figure 1C).[19–20] These inhibitors were designed to maximize the protease-inhibitor interaction and promote extensive hydrogen bond interactions with PR backbone in the structure guided strategy pioneered for darunavir.[21] Inhibitor **2** was designed with an enhanced functional group at P1′ and demonstrated to form new interactions with Gly27′ and Arg8 in the S1′ subsite.[19] Inhibitor **2** was as potent as all FDA approved drugs against wild-type PR, except for darunavir which is nearly 10 fold more potent. Moreover, **2** maintained near full potency against multidrug resistant HIV-1 isolates, while other clinical drugs, except for darunavir, showed 5 to 10 fold loss in potency. Inhibitor **3** was designed with a third tetrahydrofuran (THF) ring fused to the *bis*-THF ring at the P2 position of darunavir[20]. Inhibitor **3** displayed a 10 fold increase in potency over darunavir against multidrug resistant clinical HIV-1 strains.[20] Interestingly, both inhibitors introduce new interactions with the conserved Arg8 and Gly27 residues of PR. In order to elucidate the molecular basis for the excellent potency of these inhibitors against drug resistant strains, we studied the binding affinity and the crystal structures of PR20 in complexes with **2**, **3** and the clinical drug amprenavir. The crystal structures showed several conserved interactions between the PR20 complexes and corresponding wild-type complexes but also revealed diminished interactions due to mutations in PR20. The acquired knowledge will be helpful to improve strategies for attacking extremely resistant mutants.

RESULTS

Calorimetric analysis of inhibitor binding to PR20

The binding constants for the inhibitors (Table 1) were measured using isothermal titration calorimetry (ITC) by titrating PR20 with inhibitors at ~10-fold of PR20 concentration (Figure 2A and Table 1). Despite the presence of a third THF ring, the ligand dissociation constant (K_L) of **3** is similar to that reported for darunavir.[15] The K_L of amprenavir is 4.5-fold higher than that for **3**. Inhibitor **2** is the weakest binder of the set with a K_L value 5-fold higher than for amprenavir and 24-fold higher than for **3** as measured by ITC.

Inhibition studies on autoprocessing of TFR-PR20 precursor by compounds 2 and 3

We have reported previously that the autocatalytic cleavage (autoprocessing) of wild type precursor TFR-PR to give mature PR is inhibited by saquinavir, darunavir and atazanavir, but the autoprocessing of PR20 precursor TFR-PR20 is unresponsive to all the clinical inhibitors.[15] We have further studied the effect of added **2** and **3** in the culture medium on processing of the PR20 precursor (band a) to mature PR20 (band c) as shown in Figure 2B center and right panels, respectively. For comparison the effect of darunavir on processing of the wild-type precursor, TFR-PR, is shown in the left panel. We had previously reported that even 100–150 μM darunavir or amprenavir fails to inhibit processing of TFR-PR20 in the *E. coli* test system. Similarly, no inhibition of processing of TFR-PR20 is observed in the presence of **2** or **3** even at concentrations up to 100 μM, and thus neither of these inhibitors provides any advantage over darunavir for inhibition of PR20 precursor maturation.

The overall crystal structure

PR20 was crystallized in complex with amprenavir and the new potent antiviral inhibitors **2** and **3**. The crystallographic data collection and refinement statistics are summarized in Table 2. The crystals, which are in the orthorhombic space group $P2_12_12_1$, diffracted to high resolutions of 1.3 to 1.8 Å and refined to R-factors of 16.8 to 20%. One PR20 homodimer with residues numbered 1–99 and 1′-99′ is in the asymmetric unit of each crystal. The three inhibitors and the 20 mutations were unambiguously visible in the electron density maps, as shown by examples in Figure 1. The twenty mutations are distributed throughout the PR tertiary structure (Figure 1D). The salient structural features of PR20 identified in the PR20/darunavir and PR20/saquinavir inhibitor complexes[16] and attributed to mutations in PR20 also appear in the new PR20 complex structures. For example, the L10F mediated breakage of inter-monomer ion pair between Arg8-Asp29′ and Arg8′-Asp29[16] is observed in all three complexes with the exception of a minor conformation of Arg8 in PR20/**2** retaining an ion pair with Asp29′.

Second binding site for amprenavir

Apart from the inhibitor bound at the active site, a second inhibitor molecule of 0.7 occupancy was visible bound to one flap in the PR20/amprenavir complex. This is the first crystal structure showing amprenavir bound in a second site resembling the flap location of the second darunavir reported in the PR20/darunavir (3UCB) and PR_{V32I}/darunavir (2HS1) complexes16, 22 and consistent with kinetic data.[23] The backbone and P2′ side chain of amprenavir and darunavir share very similar conformations in their PR20 complexes, and most of the conformational variation occurs for the P1′, P1 and P2 groups (Figure 3A). All the polar contacts with protein are conserved for darunavir and amprenavir bound in the second site of PR20. The P2′ aniline group has a van der Waals contact with the carbonyl of Val56′ while the P1′ forms van der Waals interactions with the carbonyl oxygen atoms of Lys55′ and Val77′.) The second amprenavir observed at one flap of PR20 is surrounded by

3 symmetry related PR20 molecules (Figure 3B). The P2 and P2′ groups of amprenavir form extensive van der Waals contacts with one of the symmetry related PR20 molecules, while the P1 residue has van der Waals contacts with a second symmetry related PR20. The third symmetry related molecule has one van der Waals contact with the P2 group of amprenavir. Raw ITC data for APV gave an N value of ~0.8, consistent with titration by ≤1 equivalent of APV, possibly due to underestimation of its concentration. The existence of crystal lattice contacts taken together with the close to 1:1 binding stoichiometry observed in ITC indicates that the amprenavir binds only weakly to the second flap binding site and may be an artifact due to crystal packing.

Expanded S2/S2′ pocket of PR20 associated with lower inhibition by amprenavir

The PR20/amprenavir complex superimposes on the wild-type PR/amprenavir structure (3NU3) with the relatively high root mean square deviation (RMSD) of 1.07 Å for 198 equivalent Cα atoms. In contrast to the wild-type complex, amprenavir binds PR20 in a single orientation, which coincides with the minor conformation in the wild-type PR structure. All the ionic interactions observed between amprenavir and the wild-type PR are retained in the PR20/amprenavir complex, except that the direct hydrogen bond of the minor conformation of the P2′ group with the side chain of Asp30′ in the PR/amprenavir structure is replaced by a water-molecule mediated interaction in the PR20/amprenavir complex. Comparison with the PR/amprenavir structure reveals that mutations D30N, V32I, I47V and I84V in PR20 alter the size, shape and charge of the S2/S2′ pocket in the PR20/amprenavir complex as described previously for the PR20/darunavir and PR20/saquinavir (3UFN) complexes.[16] The expanded pockets are demonstrated by the increased distance of ~ 1.5/1.2 Å between the two mutated residues I47/47′V and I84/84′V on either side of the S2/S2′ pocket in the two monomers of PR20/amprenavir relative to the wild-type PR structure (Figures S1A, S1B). Also, mutations in the 80's loop have been shown to alter the potency of protease inhibitors significantly.[24]

The P2′ aniline of amprenavir in the PR20 complex shifts by ~0.6 Å to form hydrophobic contacts with the shorter valine side chain of mutation I84′V in comparison to both major and minor P2′ conformations in the wild-type PR/amprenavir complex (Figure 4A). I84′V forms two hydrophobic interactions with the aniline in the PR20/amprenavir instead of one in the wild-type complex. Also, the P2 THF ring of amprenavir in the PR20 complex is shifted by ~ 0.5 Å to form van der Waals interactions with the mutated Val84 in comparison to the major conformation of P2 THF in wild-type PR/amprenavir (Figure 4B). In contrast, the THF ring in the PR20 complex is shifted towards the I47V mutation in comparison with the position in the wild-type PR complex (Figure 4C). In addition, amprenavir in its PR20 complex lacks 1 to 3 van der Waals contacts observed between Ile84/84′ and the P1/P1′ group of amprenavir in the wild-type PR complex (Figure 4A and B). Unlike PR20/amprenavir, the single mutant PR_{I84V}/amprenavir complex retained van der Waals contacts to P1/P1′ similar to wild-type PR/amprenavir.[25] Thus, the shifts in the P2 and P2′ residues of amprenavir due to the expanded S2/S2′ pocket of PR20 add an additional interaction to I84/84′ at the expense of eliminating interactions between I84/84′V and P1′/P1 residues. The shorter side chain of I47V mutation in the PR20/amprenavir complex removes interactions of the side chain with the P2 THF ring of amprenavir (Figure 4C) but its contact with the P2′ aniline group is retained. In addition, the smaller I84V mutation results in the loss of the van der Waals contact seen between the sulfonyl oxygen of amprenavir and Ile 84′ of wild-type PR. The loss of several interactions between amprenavir and the S2/S2′ mutations in the PR20 complex shows that the P2 and P2′ groups fit loosely in the expanded S2/S2′ pocket. In the S2′ subsite, the mutated Asn30′ of PR20 forms a hydrogen bond to the mutated side chain of Asp88′ in addition to a water-molecule mediated hydrogen bond to P2′ aniline of amprenavir (Figure 4D, E). Thus, mutation N88D may compensate for the

change due to D30N mutation in the active site cavity of PR20. The wild-type PR/amprenavir complex lacks a hydrogen bond interaction between Asp30 and Asn88 in both major (Figure 4D) and minor (Figure 4E) conformations.

The amprenavir complex of PR20 can be compared with the corresponding complex with the HIV-2 protease (PR2/amprenavir) (3S45).[26] The wild type enzymes from HIV-1 and HIV-2 share 39–48% sequence identity; however, several of the mutations in PR20 exist in the wild type PR2 sequence including V32I and I47V in the S2/S2′ subsites. The PR20 and PR2 complexes share similar polar interactions with amprenavir except for those of the aniline group. In PR2/amprenavir, the aniline group lacks the hydrogen bonds to the main chain amide and carbonyl group of Asp 30′ but gains a hydrogen bond with the Asp30′ side chain consistent with its 15 fold poorer inhibition by amprenavir in comparison to wild-type HIV-1 PR[26]. However, PR20/amprenavir does not show such dramatic change in interactions with the aniline group and is very similar to wild-type HIV-1 PR/amprenavir complex, except for the shifts at the P2 and P2′ groups and the changes in hydrophobic contacts between amprenavir and PR20 (Figure 4F).

Amprenavir and darunavir differ only in the number of THF rings at the P2 position. Darunavir with its two THF rings forms more hydrogen bond interactions with the wild-type PR and binds tighter to wild-type PR than amprenavir with a single THF ring. The PR20/amprenavir complex superimposes well with the previously determined PR20/darunavir complex (3UCB) with a RMSD of 0.4 Å. The amprenavir complex lacks the two additional hydrogen bond interactions with Asp29 together with new van der Waals interactions formed by the second THF ring of darunavir. The increase in size and the loss of charge in the S2 pocket of PR20 causes the THF ring of amprenavir to shift towards I84V resulting in an elongated C-H…O interaction (from 3.3 to 3.6 Å) with the flap residue Gly48 compared to the wild-type PR. Thus, the single THF group of amprenavir does not fill the expanded S2/S2′ pocket of PR20 thereby reducing the susceptibility of the enzyme to this clinical inhibitor.

P1′-pyrrolidinone has fewer interactions with PR20 than with PR

The HIV-1 PR inhibitor **2** incorporates methyl-2-pyrrolidinone as the P1′ ligand, which was shown to interact with the Gly27′ carbonyl oxygen and Arg8 side chain in the S1′ subsite of wild-type PR.[19] Inhibitor **2** has potent activity against various drug resistant clinical isolates.[27] It retains inhibition of PR mutants bearing single substitutions associated with drug resistance.[28] The PR20/**2** complex superimposes with the previously determined wild-type PR/**2** complex[19] (3H5B) with a relatively large RMSD of 1.14 Å for 198 Cα atoms. The overall structure of PR20/**2** is more similar to the other structures of PR20/amprenavir and PR20/**3** with RMSD values of 0.51 and 0.56 Å, respectively. Unlike the wild-type PR structure where inhibitor **2** binds in two conformations, the inhibitor binds to PR20 in a single conformation resembling the major conformation in the wild-type PR complex.

When compared with amprenavir and darunavir, the P2′ position of **2** differs in the substitution of the oxymethyl group for the amino group in the aniline moiety (Figure 1). The P2′ methoxy oxygen of **2** forms hydrogen bond interactions with main chain amide groups of Asp30′ and Asn30′ in wild-type PR and PR20 complexes, respectively (Figure 5A). The methoxy methyl of the inhibitor also forms a van der Waals interaction with the side chain oxygen of Asp30′ and Asn30′ in both complexes. Thus, the methoxy substitution in **2** retains similar interactions with both Asp30′ and mutated Asn30′. Also, the PR20 structure does not show the dynamic side chain positions of Asn30 observed in various D30N single[29] and double mutants like D30N/N88D and D30N/N88S.[30] The side chain of Asn30′ in PR20/**2** complex forms a polar interaction with the side chain of mutated Asp88′

as described for other PR20 complexes (Figure 5A). The P2 group of **2** makes similar interactions with both PR20 and wild-type PR. However, unlike in the S2′ subsite, the Asn30 side chain in the S2 pocket of PR20/**2** does not form a hydrogen bond interaction with Asp88 (Figure S1C).

The P1′ group incorporates the major design change in **2**. In the wild-type PR/**2** structure, the P1′-pyrrolidine ring is visible in two alternative conformations with equal occupancy and related by 18′ rotation around the C12-C13 bond (Figure 5B).[19] In the first conformation, P1′-pyrrolidinone has a hydrogen bond between the NH and the carbonyl oxygen of Gly27. A water-molecule mediated hydrogen bond is formed between the pyrrolidinone carbonyl and the side chain of Arg8. The second conformation of P1′-pyrrolidinone has hydrophobic and C-H…O interactions with Pro81′ and Val82′. In comparison, the P1′ pyrrolidinone of PR20/**2** occurs in a single conformation similar to the first conformation seen in the wild-type PR structure and forms a hydrogen bond with the carbonyl of Gly27′. However, the P1′-pyrrolidinone in PR20 does not form the water-molecule mediated hydrogen bond with the side chain of Arg8 presumably due to the L10F mutation (Figure 5B). The L10F mutation facilitates flipping of the Arg8 side chain to form van der Waals contacts with the bulky Phe10 side chain, which breaks the intersubunit ion pair between Arg8 and Asp29′. The second conformation of P1′-pyrrolidinone is likely not favored in the PR20/**2** structure due to the I54L mutation, which displaces Pro81′ by ~1.6 Å eliminating its potential interactions with the second P1′ conformation found in the wild type PR complex (Figure 5C). Thus, changes due to PR20 mutations L10F and I54L may correlate with the higher K_L value for inhibitor **2** relative to the related PIs lacking the P1′-pyrrolidinone.

The P2 *tris*-THF in 3 adds new interactions with PR20

The potent HIV-1 PR inhibitor was developed by structure based design.[20] The major difference from darunavir is the presence of a third THF ring in **3** instead of the *bis*-THF group in the P2 position of darunavir. This larger P2 group was designed to provide additional interactions and fill the S2 pocket in wild-type PR more effectively.[20] Also, similar to **2**, the P2′ amino group in the aniline moiety is substituted with an oxymethyl group. Biological testing showed that **3** had 10-fold higher antiviral potency than darunavir against a set of drug resistant strains.[20] Studies of PR with single mutations, however, suggested **3** would be less effective on variants with the I50V mutation.[31] Superposition of the PR20/**3** complex with the wild type PR/**3** (3OK9) dimer gave a significant RMSD of 1.0 Å for 198 equivalent Cα atoms. Overall, the PR20/**3** complex is very similar to the PR20/amprenavir and PR20/**2** complexes and can be superimposed with lower RMSD values of 0.31 and 0.56 Å, respectively, for all Cα atoms. Inhibitor **3** binds in the active site of wild-type PR in two orientations related by 180′ with relative occupancies of 0.55/0.45.[20] In the PR20/**3** complex, the inhibitor binds in a single orientation similar to the major orientation in the wild-type PR complex. The interactions of the P1 and P1′ groups of the inhibitor are similar in both the wild-type and PR20 complexes. Similar to inhibitor **2**, the P2′ position of **3** has the longer oxymethyl group substituted for the amino group in the aniline moiety of amprenavir (Figure 1). Also, the P2′ methoxy oxygen of **3** forms hydrogen bond interactions with main chain amides of Asp30′ and Asn30′ in wild-type PR and PR20 complexes, respectively (Figure 6A). The methoxy methyl of the inhibitor forms a van der Waals interaction with the side chain oxygen Asn30′ in the PR20 complex similar to the van der Waals contact with the side chain of Asp30′ observed in the wild-type PR complex. The Asn30′ side chain in the PR20 complex also forms a hydrogen bond interaction with the mutated side chain of Asp88′, which does not occur in wild type PR. Thus, similar to inhibitor **2**, the extended oxymethyl group in **3** maintains Asn30′ in a single conformation that interacts with the inhibitor and Asp88′ mutated side chain.

The critical difference between amprenavir, darunavir and **3** is the presence of one, two and three THF rings at the P2 positions, respectively. The conformation and interactions of the first two THF rings of **3** are very similar in its complexes with wild-type PR and PR20. The first THF oxygen forms a hydrogen bond interaction with Asp30 and Asn30 in the wild-type PR and PR20 complexes, respectively. The Asp30 in wild-type PR exhibits two alternate conformations with the major conformation interacting with the first THF group. The majority of differences in inhibitor interactions between PR20/**3** and the wild-type PR complex are confined to the interactions of the third THF ring. In the wild-type PR complex, the presence of the third THF ring drives the carbonyl of the flap residue Gly48 into two alternate conformations with the major conformation forming a C-H…O interaction with the third THF ring in addition to the van der Waals contact to the P1 phenyl group (Figure 6B). The minor conformation of Gly48 forms van der Waals interactions with all three THF rings. Gly48 carbonyl has a single conformation in the PR20 complex, probably due to the expanded S2 subsite, and retains interactions similar to the minor conformation in the wild-type PR structure. In the wild-type PR complex, the oxygen of the third THF forms a water mediated hydrogen bond with the guanidinium group of Arg8′ and also van der Waals contacts with Arg8′. In the PR20 complex, the third THF ring has lost these interactions since the Arg8′ side chain moves to form hydrophobic interactions with the mutated side chain of L10′F (Figure 6C). However, the third THF ring in the PR20 complex retains all the van der Waals interactions with Asp29 observed in the wild-type complex. Also, the water-molecule mediated hydrogen bond interactions between the oxygen of the third THF ring and main chain carbonyl oxygens of Thr26 and Gly27 in the characteristic catalytic triplet (Asp25-Thr26-Gly27) of aspartic proteases and the water-molecule mediated interactions with the side chains of Asp29 and Arg87 are conserved in both the wild-type and PR20 complexes (Figure 6C). The two water molecules involved in these interactions are internal structural water molecules conserved in the majority of PR structures.[32] Further, the third THF ring in the PR20 complex packs neatly against the P1 phenyl group of the inhibitor as described for the wild-type complex and retains good internal hydrophobic contacts that cannot occur for the single or *bis*-THF group in amprenavir and darunavir, respectively. Thus, despite the new interactions of the P2 group of inhibitor **3**, some of the interactions with Arg8 and to the flap are lost in the PR20 complex, resulting in binding affinity similar to that of darunavir for PR20.

DISCUSSION AND CONCLUSIONS

We propose that PR20 provides a useful model for evaluation and development of new inhibitors targeting emerging strains of multidrug resistant virus. Recently, we characterized the structural changes in the clinically derived extreme drug resistant protease PR20 bearing 20 mutations.[16] PR20 showed substantially lower affinity for PIs by > 3 orders of magnitude relative to wild type PR.[15] Analysis of ITC data shows that the markedly lower affinity of PR20 for darunavir of 10^4-fold arises primarily from a ΔH that is significantly less favorable by 4.5 kcal/mol accompanied by a small (~0.5 kcal/mol) unfavorable decrease in the entropic effect (less negative $-T\Delta S$) relative to the corresponding wild type values. Amprenavir exhibits a ~500-fold lower affinity for PR20 relative to wild-type PR, due to unfavorable changes of 1.5 and 1.7 kcal/mol in ΔH and $-T\Delta S$ respectively.[33] Overall, energy contributions to binding of darunavir, 1 and structurally related inhibitors to PR20 are predominantly enthalpic, unlike the large change in entropy reported recently for binding to different mutants.[34]

In addition, the autocatalytic cleavage of PR20 precursor to release mature protease is not inhibited significantly by the clinical PIs, although the autoprocessing of wild-type PR precursor is inhibited effectively by darunavir and saquinavir.[15, 35–36] Our studies show that

2 and **3**, like the clinical inhibitors, do not inhibit the autocatalytic cleavage of PR20 precursor.

The new crystal structures of PR20 in complex with amprenavir, **2** and **3** reveal the molecular mechanisms for evasion of these inhibitors. Amprenavir has the smallest P2 group among these three inhibitors, which appears to fit poorly in the expanded S2 pocket of PR20 consistent with 4-fold weaker affinity relative to darunavir. Inhibitor **2** has the weakest affinity for PR20 probably due to poorer interaction of the P1′ moiety in PR20 compared with wild-type PR. The highest affinity for PR20 was shown by **3** since its bulky *tris*-THF rings fill the expanded hydrophobic S2 pocket of PR20 more effectively than do the smaller P2 groups in the other two inhibitors. However, despite the addition of a third THF ring, the K_L values of **3** and darunavir are almost identical. The favorable affinity of **3** for PR20 agrees with its high antiviral potency.[20] In fact, **3** exhibits 10-fold higher potency than darunavir on tested multidrug resistant viral strains, which may reflect different effects in the cell compared to the isolated protein. Overall, **3** is a promising inhibitor for further development against extreme drug resistant variants exemplified by PR20. Structural analysis suggests inhibitors may be improved by adding more polar interactions with the flexible flaps, as well as increasing the size of P2/P2' groups. Preventing the L10F mediated breakage of the ion pair between Arg8/8′ and Asp29′/29 may be important for stronger inhibition of PR20. The insertion between L10F and Arg8 of the P2 group of saquinavir from the second binding site in the PR20/saquinavir complex[16] may suggest a possible approach to overcome the effects of the L10F mutation.

EXPERIMENTAL SECTION

General

Inhibitor **2** has shown analytical purity >99% by HPLC analysis,[28] and inhibitor **3** has shown analytical purity of >98% by HPLC[31]. The structures were confirmed by ^{1}H and ^{13}C NMR spectral analysis, and high resolution mass spectrometry. For inhibitor **2** HRMS (*m/z*) calcd for C30H40N3O8S [M+H]+ 602.2536, found 602.2536. For inhibitor **3** HRMS (ESI) [M+Na]+ calcd for C30H40N2O9SNa: 627.2352, found: 627.2359.

Construction, Expression and purification of PR20

A 99 amino acid synthetic gene termed PR20 derived from the protease sequence of a clinical isolate[37] was cloned between the Nde1 and BamH1 sites of pET11a vector (Novagen, San Diego, CA) and transformed into *E.coli* BL-21(DE3; Stratagene). Protein expression, purification and folding were carried out as described previously.[38]

In vivo autoprocessing of TFR-PR20 in *E. coli*

Precursor construct TFR-PR20 comprising the multidrug resistant PR20 sequence fused to the full length TFR was cloned and expressed in *E. coli,* and the effect of added inhibitors to inhibit autoprocessing was assessed by growing the cultures in the presence of increasing concentrations of **3** and **2** in the medium. The expressed protein was partially purified and analyzed by SDS-PAGE as described and compared to the wild-type TFR-PR construct inhibited by darunavir.[15]

Isothermal Titration Calorimetry

PR20 (53 μL of a 1.8–2.15 mg/mL solution in 12 mM HCl) was folded by addition of 5 mM sodium acetate buffer, pH 6 (buffer A), to give 175 μL, followed immediately by 175 μL of 100 mM sodium acetate buffer, pH 5 (Buffer B), and centrifuged for 2–4 min at 16,000 × g. The supernatant was transferred to the calorimeter cell (MicroCal high-precision iTC_{200}

microcalorimeter, GE Healthcare) and titrated as described[15] with inhibitors at ~10-fold the PR20 concentration in a buffer of the same composition. Data were analyzed by use of the Origin software provided with the instrument. Since it was not possible to determine accurately the concentrations of the **2** and **3** inhibitors because of the limited amounts available, inhibitor concentrations were estimated from the observed N values at known PR20 concentration and an active site binding stoichiometry of 1:1 inhibitor:PR20, to give corrected N values of 1.0. For consistency the same correction procedure was also used for darunavir and amprenavir.

Crystallization, X-ray data collection and structure determination

The inhibitors amprenavir, **2**, and **3** were mixed with PR20 at a 5:1 molar ratio and incubated on ice for 30 minutes prior to crystallization trials. The complexes were crystallized by the hanging drop vapor diffusion technique at room temperature. The PR20/amprenavir crystals were grown by mixing 1 μl of protein complex (5 mg/ml) and 1 μl of reservoir solution well solution containing 1.67M sodium chloride and 67mM citrate-phosphate buffer at pH 4.2. The reservoir used for growing PR20/**2** was 1.2M lithium chloride and 0.1 M sodium acetate at pH 4.8. The PR20/**3** complex crystals were obtained with well solution containing 0.25M potassium iodide and 0.1M sodium acetate buffer at pH 4.8. The cryoprotectant for crystals was composed of 30% glycerol and the respective mother liquor. Diffraction data at 100 °K were collected on beamline 22-ID (SER-CAT) at the Advance Photon Source, Argonne National Laboratory (Argonne, Il, USA). All data were integrated and scaled with HKL2000.[39]

The crystal structures were solved by molecular replacement using Phaser.[40–41] The PR dimer from the crystal structure of PR_{I50V}/darunavir (2F8G)42 was used as the search model for the PR20/amprenavir complex. For PR20/**2** and PR20/**3** complexes, the search model was the PR dimer from PR_{M46L}/darunavir (2HS2)22. The atomic models were refined by iterative rounds of model building into electron density maps and refinement using COOT[43], REFMAC[44] (PR20/amprenavir) and SHELX-97[45] (PR20/**2** and PR20/**3**). The surface loops including 10's, 30's and 60's loops with ambiguous densities were pruned during early stages of refinement and successfully rebuilt. The correct amino acid side chain corresponding to the 20 mutations were adding during the refinement. The three inhibitors were fitted into unambiguous electron densities of the respective structures. Solvent molecules were inserted at stereochemically reasonable positions using 2Fo-Fc and Fo-Fc maps contoured at 1 and 3 sigma levels, respectively. The hydrogen bond interaction is defined by a distance in the range of 2.6–3.5 Å between hydrogen donor and acceptor atoms. The C-H…O interaction has a C…O distance of 3.0–3.7 Å.[47] The van der Waals interaction has C-H…H-C distance of 3.8–4.2 Å.[46] Molecular figures were prepared with PyMOL (http://www.pymol.org).

Supplementary Material

Refer to Web version on PubMed Central for supplementary material.

Acknowledgments

The research was supported in part by the National Institute of Health grants GM062920 (I.T.W.) and GM053386 (A.K.G.) and by the Georgia State University Molecular Basis of Disease Fellowship and the Georgia State University Research Program Enhancement Award in Bioinformatics (C.-H.S.), and by the Intramural Research Program of the NIDDK and the Intramural AIDS-Targeted Antiviral Program of the Office of the Director, NIH. This research was authored, in whole or in part, by National Institutes of Health staff. Data were collected at the Southeast Regional Collaborative Access Team (SER-CAT) beamline 22ID at the Advanced Photon Source, Argonne National Laboratory. Supporting institutions may be found at www.ser-cat.org/members.html.

Amprenavir and darunavir were obtained through the NIH AIDS Research and Reference Reagent Program, Division of AIDS, NIAID, NIH.

ABBREVIATIONS USED

APV	amprenavir
DRV	darunavir
HIV-1	human immunodeficiency virus type 1
HAART	highly active antiretroviral therapy
ITC	isothermal titration calorimetry
PR	mature HIV-1 protease
PI	clinical inhibitor of PR
***tris*-THF**	*tris*-tetrahydrofuran
PDB	Protein Data Bank
RMSD	root mean square deviation

References

1. Sepkowitz KA. AIDS--the first 20 years. N Engl J Med. 2001; 344:1764–1772. [PubMed: 11396444]
2. Condra JH, Schleif WA, Blahy OM, Gabryelski LJ, Graham DJ, Quintero JC, Rhodes A, Robbins HL, Roth E, Shivaprakash M, et al. In vivo emergence of HIV-1 variants resistant to multiple protease inhibitors. Nature. 1995; 374:569–571. [PubMed: 7700387]
3. Mehellou Y, De Clercq E. Twenty-six years of anti-HIV drug discovery: where do we stand and where do we go? J Med Chem. 2010; 53:521–538. [PubMed: 19785437]
4. Menendez-Arias L. Molecular basis of human immunodeficiency virus drug resistance: an update. Antiviral Res. 2010; 85:210–231. [PubMed: 19616029]
5. Grubb JR, Singhatiraj E, Mondy K, Powderly WG, Overton ET. Patterns of primary antiretroviral drug resistance in antiretroviral-naive HIV-1-infected individuals in a midwest university clinic. AIDS. 2006; 20:2115–2116. [PubMed: 17053358]
6. Liao L, Xing H, Dong Y, Qin G, Ma Y, Lu H, Chen L, Zhang L, Osborne C, Seguy N, Wei D, Sun F, Yang J, Ruan Y, Shao Y. Surveys of Transmitted HIV Drug Resistance in 7 Geographic Regions in China, 2008–2009. Clin Infect Dis. 2012; 54 (Suppl 4):S320–323. [PubMed: 22544196]
7. Hunt GM, Ledwaba J, Basson AE, Moyes J, Cohen C, Singh B, Bertagnolio S, Jordan MR, Puren A, Morris L. Surveillance of Transmitted HIV-1 Drug Resistance in Gauteng and KwaZulu-Natal Provinces, South Africa, 2005–2009. Clin Infect Dis. 2012; 54 (Suppl 4):S334–338. [PubMed: 22544199]
8. Duc NB, Hien BT, Wagar N, Tram TH, Giang le T, Yang C, Wolfe MI, Hien NT, Tuan NA. Surveillance of Transmitted HIV Drug Resistance Using Matched Plasma and Dried Blood Spot Specimens From Voluntary Counseling and Testing Sites in Ho Chi Minh City, Vietnam, 2007–2008. Clin Infect Dis. 2012; 54 (Suppl 4):S343–347. [PubMed: 22544201]
9. Hamers RL, Wallis CL, Kityo C, Siwale M, Mandaliya K, Conradie F, Botes ME, Wellington M, Osibogun A, Sigaloff KC, Nankya I, Schuurman R, Wit FW, Stevens WS, van Vugt M, de Wit TF. HIV-1 drug resistance in antiretroviral-naive individuals in sub-Saharan Africa after rollout of antiretroviral therapy: a multicentre observational study. Lancet Infect Dis. 2011; 11:750–759. [PubMed: 21802367]
10. Sigaloff KC, Mandaliya K, Hamers RL, Otieno F, Jao IM, Lyagoba F, Magambo B, Kapaata A, Ndembi N, Rinke de Wit TF. High Prevalence of Transmitted Antiretroviral Drug Resistance Among Newly HIV Type 1 Diagnosed Adults in Mombasa, Kenya. AIDS Res Hum Retroviruses. 2012

11. Jordan MR, Bennett DE, Wainberg MA, Havlir D, Hammer S, Yang C, Morris L, Peeters M, Wensing AM, Parkin N, Nachega JB, Phillips A, De Luca A, Geng E, Calmy A, Raizes E, Sandstrom P, Archibald CP, Perriens J, McClure CM, Hong SY, McMahon JH, Dedes N, Sutherland D, Bertagnolio S. Update on World Health Organization HIV Drug Resistance Prevention and Assessment Strategy: 2004–2011. Clin Infect Dis. 2012; 54 (Suppl 4):S245–249. [PubMed: 22544182]
12. Hirsch MS, Gunthard HF, Schapiro JM, Brun-Vezinet F, Clotet B, Hammer SM, Johnson VA, Kuritzkes DR, Mellors JW, Pillay D, Yeni PG, Jacobsen DM, Richman DD. Antiretroviral drug resistance testing in adult HIV-1 infection: 2008 recommendations of an International AIDS Society-USA panel. Clin Infect Dis. 2008; 47:266–285. [PubMed: 18549313]
13. Heneine W, Kashuba A. HIV Prevention by Oral Preexposure Prophylaxis. Cold Spring Harb Perspect Med. 2012; 2:a007419. [PubMed: 22393535]
14. Supervie V, Garcia-Lerma JG, Heneine W, Blower S. HIV, transmitted drug resistance, and the paradox of preexposure prophylaxis. Proc Natl Acad Sci U S A. 2010; 107:12381–12386. [PubMed: 20616092]
15. Louis JM, Aniana A, Weber IT, Sayer JM. Inhibition of autoprocessing of natural variants and multidrug resistant mutant precursors of HIV-1 protease by clinical inhibitors. Proc Natl Acad Sci U S A. 2011; 108:9072–9077. [PubMed: 21576495]
16. Agniswamy J, Shen CH, Aniana A, Sayer JM, Louis JM, Weber IT. HIV-1 Protease with 20 Mutations Exhibits Extreme Resistance to Clinical Inhibitors through Coordinated Structural Rearrangements. Biochemistry. 2012; 51:2819–2828. [PubMed: 22404139]
17. Flexner C. HIV drug development: the next 25 years. Nat Rev Drug Discov. 2007; 6:959–966. [PubMed: 17932493]
18. Williams GC, Sinko PJ. Oral absorption of the HIV protease inhibitors: a current update. Adv Drug Deliv Rev. 1999; 39:211–238. [PubMed: 10837775]
19. Ghosh AK, Leshchenko-Yashchuk S, Anderson DD, Baldridge A, Noetzel M, Miller HB, Tie Y, Wang YF, Koh Y, Weber IT, Mitsuya H. Design of HIV-1 protease inhibitors with pyrrolidinones and oxazolidinones as novel P1'-ligands to enhance backbone-binding interactions with protease: synthesis, biological evaluation, and protein-ligand X-ray studies. J Med Chem. 2009; 52:3902–3914. [PubMed: 19473017]
20. Ghosh AK, Xu CX, Rao KV, Baldridge A, Agniswamy J, Wang YF, Weber IT, Aoki M, Miguel SG, Amano M, Mitsuya H. Probing multidrug-resistance and protein-ligand interactions with oxatricyclic designed ligands in HIV-1 protease inhibitors. ChemMedChem. 2010; 5:1850–1854. [PubMed: 20827746]
21. Ghosh AK, Anderson DD, Weber IT, Mitsuya H. Enhancing protein backbone binding--a fruitful concept for combating drug-resistant HIV. Angew Chem Int Ed Engl. 2012; 51:1778–1802. [PubMed: 22290878]
22. Kovalevsky AY, Liu F, Leshchenko S, Ghosh AK, Louis JM, Harrison RW, Weber IT. Ultra-high resolution crystal structure of HIV-1 protease mutant reveals two binding sites for clinical inhibitor TMC114. J Mol Biol. 2006; 363:161–173. [PubMed: 16962136]
23. Kovalevsky AY, Ghosh AK, Weber IT. Solution kinetics measurements suggest HIV-1 protease has two binding sites for darunavir and amprenavir. J Med Chem. 2008; 51:6599–6603. [PubMed: 18808097]
24. Mahalingam AK, Axelsson L, Ekegren JK, Wannberg J, Kihlstrom J, Unge T, Wallberg H, Samuelsson B, Larhed M, Hallberg A. HIV-1 protease inhibitors with a transition-state mimic comprising a tertiary alcohol: improved antiviral activity in cells. J Med Chem. 2010; 53:607–615. [PubMed: 19961222]
25. Shen CH, Wang YF, Kovalevsky AY, Harrison RW, Weber IT. Amprenavir complexes with HIV-1 protease and its drug-resistant mutants altering hydrophobic clusters. FEBS J. 2010; 277:3699–3714. [PubMed: 20695887]
26. Tie Y, Wang YF, Boross PI, Chiu TY, Ghosh AK, Tozser J, Louis JM, Harrison RW, Weber IT. Critical differences in HIV-1 and HIV-2 protease specificity for clinical inhibitors. Protein Sci. 2012; 21:339–350. [PubMed: 22238126]

27. Koh Y, Das D, Leschenko S, Nakata H, Ogata-Aoki H, Amano M, Nakayama M, Ghosh AK, Mitsuya H. GRL-02031; a novel nonpeptidic protease inhibitor (PI) containing a stereochemically defined fused cyclopentanyltetrahydrofuran potent against multi-PI-resistant human immunodeficiency virus type 1 in vitro. Antimicrob Agents Chemother. 2009; 53:997–1006. [PubMed: 18955518]
28. Chang YC, Yu X, Zhang Y, Tie Y, Wang YF, Yashchuk S, Ghosh AK, Harrison RW, Weber IT. Potent antiviral HIV-1 protease inhibitor GRL-02031 adapts to the structures of drug resistant mutants with its P1'-pyrrolidinone ring. J Med Chem. 2012; 55:3387–3397. [PubMed: 22401672]
29. Kozisek M, Bray J, Rezacova P, Saskova K, Brynda J, Pokorna J, Mammano F, Rulisek L, Konvalinka J. Molecular analysis of the HIV-1 resistance development: enzymatic activities, crystal structures, and thermodynamics of nelfinavir-resistant HIV protease mutants. J Mol Biol. 2007; 374:1005–1016. [PubMed: 17977555]
30. Bihani SC, Das A, Prashar V, Ferrer JL, Hosur MV. Resistance mechanism revealed by crystal structures of unliganded nelfinavir-resistant HIV-1 protease non-active site mutants N88D and N88S. Biochem Biophys Res Commun. 2009; 389:295–300. [PubMed: 19720046]
31. Zhang H, Wang YF, Shen CH, Agniswamy J, Rao KV, Ghosh AK, Harrison RW, Weber IT. Novel P2 tris-tetrahydrofuran group in antiviral compound 1 (GRL-0519) fills the S2 binding pocket of selected mutants of HIV-1 protease. J Med Chem. 2013:1074–1083. [PubMed: 23298236]
32. Mahalingam B, Louis JM, Hung J, Harrison RW, Weber IT. Structural implications of drug-resistant mutants of HIV-1 protease: high-resolution crystal structures of the mutant protease/substrate analogue complexes. Proteins. 2001; 43:455–464. [PubMed: 11340661]
33. King NM, Prabu-Jeyabalan M, Nalivaika EA, Wigerinck P, de Bethune MP, Schiffer CA. Structural and thermodynamic basis for the binding of TMC114: a next-generation human immunodeficiency virus type 1 protease inhibitor. J Virol. 2004; 78:12012–12021. [PubMed: 15479840]
34. King NM, Prabu-Jeyabalan M, Bandaranayake RM, Nalam MN, Nalivaika EA, Ozen A, Haliloglu T, Yilmaz NK, Schiffer CA. Extreme Entropy-Enthalpy Compensation in a Drug-Resistant Variant of HIV-1 Protease. ACS Chem Biol. 2012; 7:1536–1546. [PubMed: 22712830]
35. Huang L, Li Y, Chen C. Flexible catalytic site conformations implicated in modulation of HIV-1 protease autoprocessing reactions. Retrovirology. 2011; 8:79. [PubMed: 21985091]
36. Davis DA, Soule EE, Davidoff KS, Daniels SI, Naiman NE, Yarchoan R. Activity of Human Immunodeficiency Virus Type 1 Protease Inhibitors Against the Initial Autocleavage in Gag-Pol Polyprotein Processing. Antimicrob Agents Chemother. 2012; 56:3620–3628. [PubMed: 22508308]
37. Dierynck I, De Wit M, Gustin E, Keuleers I, Vandersmissen J, Hallenberger S, Hertogs K. Binding kinetics of darunavir to human immunodeficiency virus type 1 protease explain the potent antiviral activity and high genetic barrier. J Virol. 2007; 81:13845–13851. [PubMed: 17928344]
38. Sayer JM, Agniswamy J, Weber IT, Louis JM. Autocatalytic maturation, physical/chemical properties, and crystal structure of group N HIV-1 protease: relevance to drug resistance. Protein Sci. 2010; 19:2055–2072. [PubMed: 20737578]
39. Otwinowski Z, Minor W. Processing of X-ray diffraction data collected in oscillation mode. Method Enzymol. 1997; 276:307–326.
40. Storoni LC, McCoy AJ, Read RJ. Likelihood-enhanced fast rotation functions. Acta Crystallogr D Biol Crystallogr. 2004; 60:432–438. [PubMed: 14993666]
41. McCoy AJ, Grosse-Kunstleve RW, Storoni LC, Read RJ. Likelihood-enhanced fast translation functions. Acta Crystallogr D Biol Crystallogr. 2005; 61:458–464. [PubMed: 15805601]
42. Kovalevsky AY, Tie Y, Liu F, Boross PI, Wang YF, Leshchenko S, Ghosh AK, Harrison RW, Weber IT. Effectiveness of nonpeptide clinical inhibitor TMC-114 on HIV-1 protease with highly drug resistant mutations D30N, I50V, and L90M. J Med Chem. 2006; 49:1379–1387. [PubMed: 16480273]
43. Emsley P, Cowtan K. Coot: model-building tools for molecular graphics. Acta Crystallogr D Biol Crystallogr. 2004; 60:2126–2132. [PubMed: 15572765]

44. Murshudov GN, Vagin AA, Dodson EJ. Refinement of macromolecular structures by the maximum-likelihood method. Acta Crystallogr D Biol Crystallogr. 1997; 53:240–255. [PubMed: 15299926]

45. Sheldrick GM, Schneider TR. SHELXL: high-resolution refinement. Methods Enzymol. 1997; 277:319–343. [PubMed: 18488315]

46. Weber, IT.; Wang, Y-F. HIV protease: role in viral replication, protein-ligand X-ray crystal structures and inhibitor design. In: Gosh, AK., editor. Aspartic Protease as Therapeutic Targets. Vol. 45. Wiley-VCH Verlag GmbH & Co; 2010. p. 109-137.

47. Panigrahi SK, Desiraju GR. Strong and weak hydrogen bonds in the protein-ligand interface. Proteins. 2007; 67:128–141. [PubMed: 17206656]

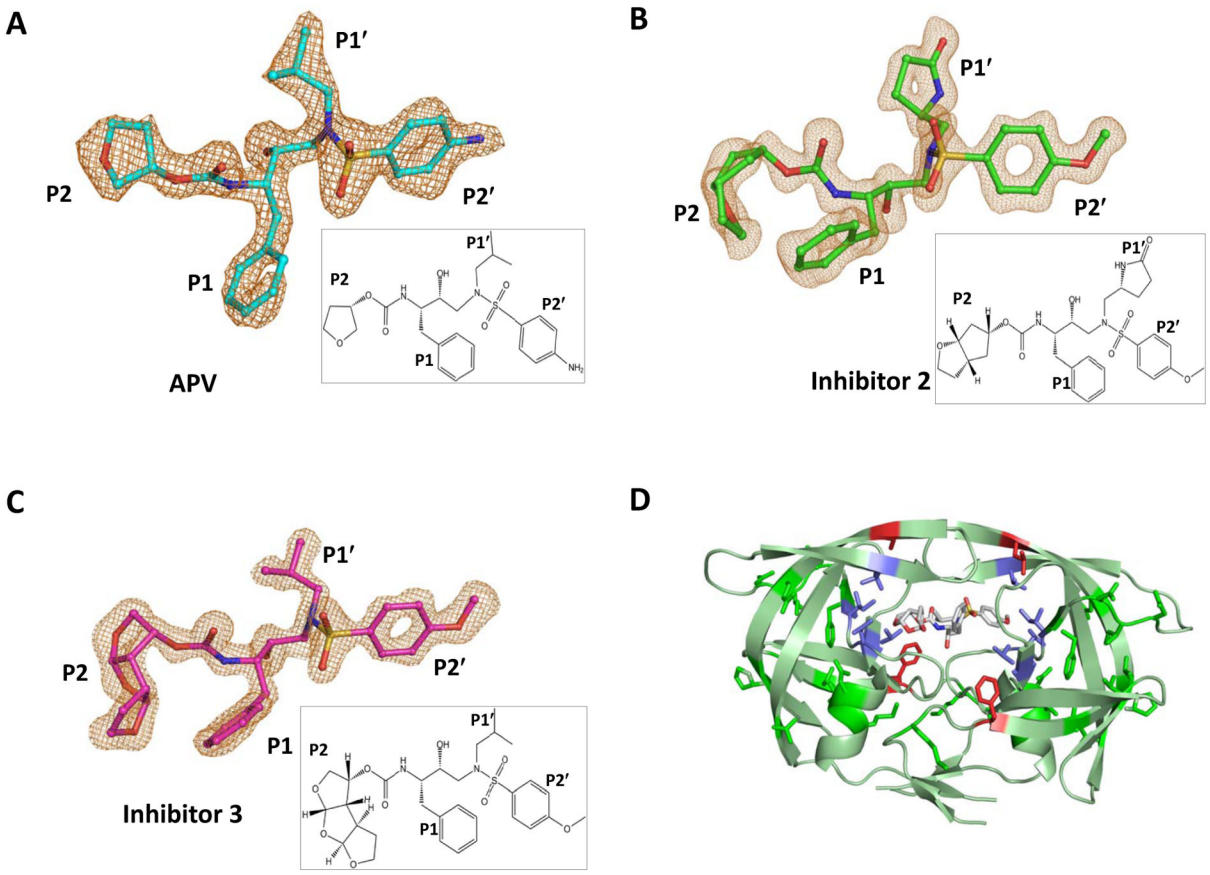

Figure 1.

F_o-F_c omit maps contoured at 3′ level for (A) amprenavir (APV), (B) inhibitor **2**, and (C) inhibitor **3**. The chemical structure of the inhibitors are shown in the inserts of panels (A), (B) and (C). (D) Sites of the 20 mutations of highly drug resistant PR20 are mapped on HIV-1 PR dimer (green cartoon representation) with the bound inhibitor **3** colored by atom type in stick representation. The mutations with direct interaction to inhibitors are shown as blue sticks, while the distal mutations are shown as green sticks, the critical L10F and I54L mutations are shown as red sticks.

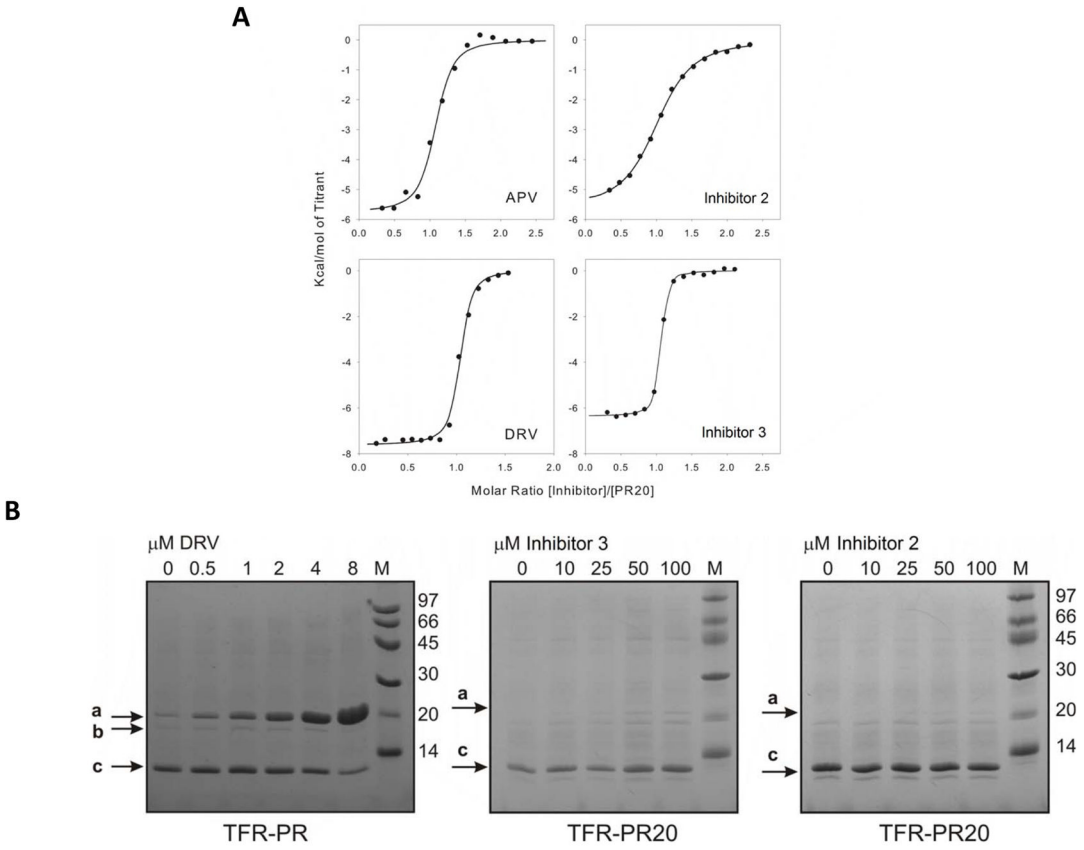

Figure 2.

(A) Calorimetric titration of PR20 with inhibitors. For conditions see Experimental Procedures. Quantitative results are tabulated in Table 1. (B) Left panel, dose-response for darunavir (DRV) inhibition of autocatalytic processing of wild type TFR-PR in the *E. coli* expression system as described in [15]. Band a, full length TFR-PR; b, cleavage product between F8/L9 within the TFR; c, mature protease. Note that virtually complete inhibition by 8 μM darunavir is accompanied by extensive buildup of the precursor. No inhibition is observed by added **3** (center panel) or **2** (right panel) on processing of the precursor TFR-PR20 to mature protease.

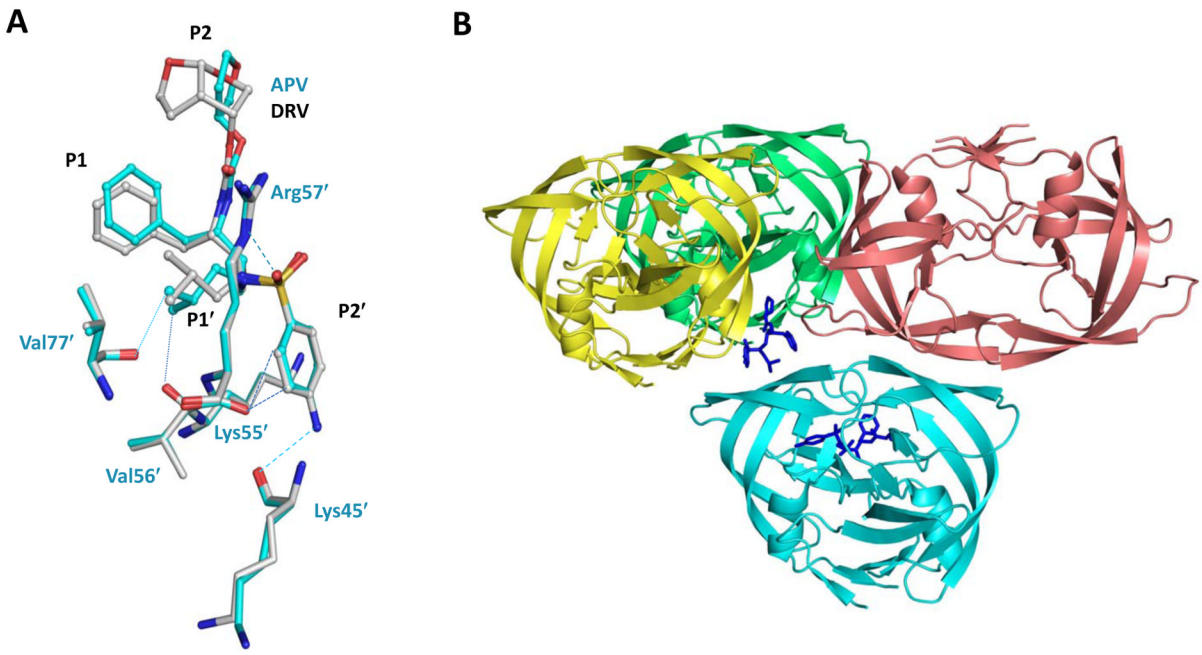

Figure 3.

(A) The second amprenavir is observed bound in the PR20/amprenavir complex (cyan carbons) at the same location as the second darunavir site seen in the PR20/darunavir complex (grey carbons). The hydrogen bonds are indicated by broken lines and van der Waals contacts as dotted lines. (B) The second amprenavir (blue sticks) binds near one flap of PR20 (cyan) forming 2 hydrogen bond interactions and several van der Waals interactions, and also has hydrophobic contacts with 3 symmetry related PR20 dimers. The P2 and P2′ groups of amprenavir form extensive van der Waals contacts with the symmetry molecule 1 (yellow) while the P1 group has van der Waals contacts with the symmetry molecule 2(pink). The symmetry molecule 3 (green) has a single van der Waals contact with the P2 group of amprenavir.

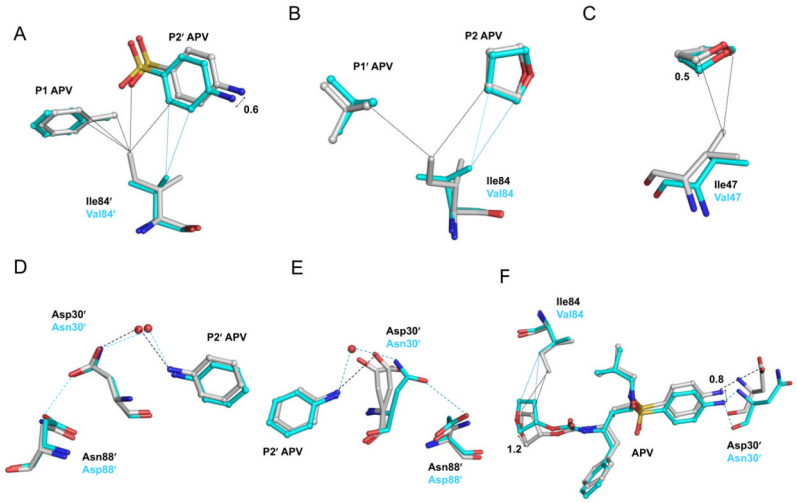

Figure 4.

Structural comparison of amprenavir (APV) complexes with PR20 (cyan carbons) and wild-type PR (grey carbons). The protein is represented in sticks while the inhibitor atoms are in ball and stick format. The hydrogen bonds are indicated by broken lines and the van der Waals contacts are in dotted lines colored cyan or black according to the complex. (A) The P2′ group of amprenavir is shifted by ~0.6 Å towards the I84V mutation in PR20 in comparison to the major conformation of amprenavir in its complex with wild-type PR (grey carbon), which also eliminates PR20 interactions with the P1 group. (B) The P2 THF group in PR20/amprenavir forms an additional van der Waals contact with the I84V side chain, while the interaction with the P1′ group is eliminated in comparison to the major conformation of amprenavir in the wild-type PR complex. (C) The P2 THF group loses van der Waals interactions with the mutated Val47 side chain in PR20/amprenavir in comparison to the major conformation of amprenavir in its wild-type PR complex. (D) The mutated Asn30 forms a water-molecule mediated interaction with P2′ and hydrogen bond interaction with the N88D mutation in PR20/amprenavir in comparison to the major conformation of amprenavir in the wild-type PR complex. (E). The direct hydrogen bond between P2′ aniline and Asp30′ in the minor conformation of wild-type PR/amprenavir is lost in PR20/amprenavir. However, the side chain of D30′N forms a hydrogen bond with N88′D in PR20/amprenavir. (F) The P2 and P2′ groups of PR20/amprenavir are shifted towards I84/84′V mutation in comparison to the PR2/amprenavir complex (grey carbons). In contrast to PR2/amprenavir, the P2′ aniline of PR20/amprenavir retains the hydrogen bonds to the main chain amide and the carbonyl of D30N similar to wild-type PR/amprenavir but lacks the hydrogen bond to the side chain of Asp30.

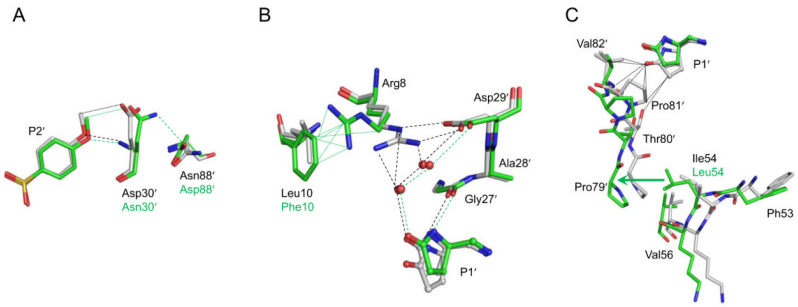

Figure 5.

Comparison of inhibitor **2** complexes with PR20 (green carbons) and wild-type PR (grey carbons). The protein is represented in sticks while the inhibitor atoms are in ball and stick format. The hydrogen bonds are indicated by broken lines, the van der Waals contacts are in dotted lines colored according to the complex. (A) The P2′ of **2** forms hydrogen bond interactions and C-H…O interaction with main chain amide and the side chain oxygen of Asp30′ and Asn30′ in wild-type PR and PR20 complexes. The D30′N mutation in PR20/**2** complex forms hydrogen bond interactions with N88′D. (B) The L10F mutation eliminates the ion pair between Arg8 and Asp29′. The critical water-molecule mediated interactions between P1′and Arg′ are also lost in the PR20/**2** complex. (C). The displacement of 80's loop by the I54L flap mutation in PR20/**2** prevents the interactions observed between Pro81′, Val82′ and the second conformation of P1′ in the wild-type PR/**2** complex.

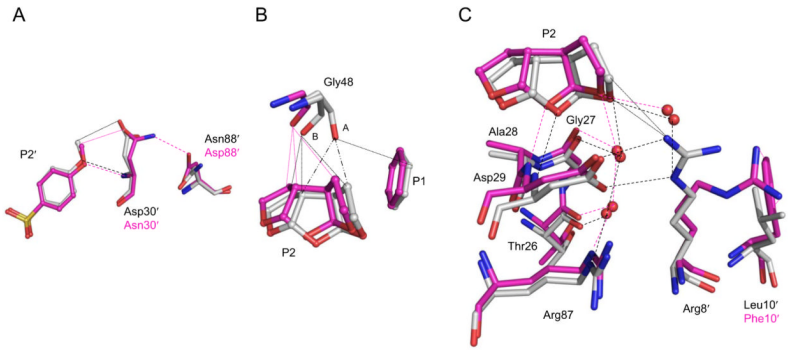

Figure 6.

Comparison of inhibitor **3** complexes with PR20 (magenta carbons) and wild-type PR (grey carbons). The protein is represented in sticks while the inhibitor atoms are in ball and stick format. The hydrogen bonds are indicated by broken lines, the van der Waals contacts are in dotted lines and the C-H…O interactions are shown as (··–··) and colored according to the complex. (A) The residue 30 forms a hydrogen bond and a C-H…O interaction with the P2′ oxymethyl group of **3** in both wild-type PR and PR20. The mutated Asn30 side chain also forms a hydrogen bond with mutated Asp88 in PR20 complex in contrast to their lack of interaction in the wild-type PR complex. (B) The flap residue Gly48 showed two alternative conformations (A and B) and different interactions with inhibitor in the wild type PR/**3** complex. In PR20/**3**, Gly48 adopts the conformation B observed in the wild-type PR complex which results in the loss of stronger C-H…O interactions with the *tris*-THF rings of **3**. In addition, the van der Waals contact with the P1 group of **3** is also lost. (C) The L10′F mediated buckling of Arg8′ in PR20 results in the loss of the ion pair with Arg29 and the loss of water-molecule mediated hydrogen bonds connecting the third THF ring and Arg8′. The van der Waals contacts between the third THF ring and Arg8′ are also not observed in the PR20/**3** complex.

Table 1

ITC data for inhibitor binding to PR20[a]

Protein	Inhibitor	K_A	K_L	ΔH	ΔS	$-T\Delta S$[b]
PR20		**M^{-1}**	**nM**	**kcal/mol**	**cal/mol/deg**	**kcal/mol**
	Darunavir	$24.5 \pm 5.9 \times 10^6$	41[c]	−7.61 ± 0.11	8.53	−2.57[d]
	Amprenavir	$5.61 \pm 1.69 \times 10^6$	178	−5.76 ± 0.17	11.8	−3.55[d]
	2	$1.04 \pm 0.07 \times 10^6$	960	−5.62 ± 0.08	8.86	−2.67[d]
	3	$25.3 \pm 5.3 \times 10^6$	39.5	−6.50 ± 0.07	12.3	−3.70[d]
PR[e]	Darunavir	3.2×10^{11}	0.0045	−12.1		−3.1[f]
	Amprenavir	2.5×10^9	0.39	−7.3		−5.3[f]

[a] K_A, ligand association constant; K_L, ligand dissociation constant ($1/K_A$).

[b] $T\Delta S$ is given in the same units to indicate the relative contribution of entropy vs. enthalpy to the overall free energy ($\Delta G = \Delta H - T\Delta S$) of ligand binding.

[c] Previously reported in[15]

[d] At 28 °C

[e] Data from[33]

[f] [d] At 20 °C

Table 2

Crystallographic data collection and refinement statistics

PR20 Complexes	PR20/amprenavir	PR20/2	PR20/3
Space group	$P2_12_12_1$	$P2_12_12_1$	$P2_12_12_1$
Cell Dimensions			
a (Å)	28.72	28.64	28.57
b (Å)	65.80	65.97	65.79
c (Å)	94.56	93.71	92.82
Resolution range	50.0 – 1.8	50.0 – 1.31	50.0 – 1.55
Unique reflections	15764	39582	24299
Redundancy	4.5 (3.1)	5.5 (2.3)	6.1 (1.8)
Completeness	97.6 (80.0)[a]	90.8 (50.1)	92.5 (50.2)
$\langle I/\sigma(I)\rangle$	19.3 (2.0)	16.2 (3.0)	22.6 (2.5)
R_{sym} (%)	7.3 (46.8)	7.6 (26.3)	6.9 (26.5)
Refinement resolution range	10 – 1.8	10.0 – 1.31	10.0–1.55
R_{cryst} (%)	19.8	16.8	20.0
R_{free} (%)	25.0	22.9	26.0
Number of solvent molecules	102	116	114
Average B-factor (Å^2)			
Main chain	21.4	17.0	16.4
Side chain	23.4	23.7	23.8
Inhibitor	32.8	14.9	11.1
Solvent	28.6	25.9	22.4
RMS deviations from ideality			
Bond length (Å)	0.02	0.01	0.01
Angles	1.8 (°)[b]	0.03 (Å)	0.03 (Å)[c]

[a] Values in parentheses are given for the highest resolution shell

[b] The angle rmsd in REFMAC 5.2 is indicated by angle in degree

[c] The angle rmsd in SHELX97 is indicated by distance in Å